Bulletin of Earth Sciences of Thailand

Relationship Between Hotspot and Geography - Meteorology Factors in Thailand and Neighboring Countries

Thanchanok Ngernted and Santi Pailoplee*

Morphology of Earth Surface and Advanced Geohazards in Southeast Asia (MESA RU),
Department of Geology, Faculty of Science, Chulalongkorn University, Bangkok 10330, Thailand

*Corresponding author e-mail: Pailoplee.S@gmail.com

Received: 05 Apr 2025
Revised: 09 Jun 2025
Accepted: 06 Jul 2025

ABSTRACT

Air pollution is a critical issue in many countries and has become a significant problem in Southeast Asia. Wildfires, agricultural burning, and biomass burning are major sources of pollution emissions. This study aims to analyze hotspot activity and examine the relationship between hotspots and geographic-meteorological factors in Thailand and neighboring countries. MODIS hotspot data were analyzed using the frequency-magnitude distribution (FMD) and geography-meteorology factors. The results indicate that areas with high hotspot activity were mainly found in northwestern to eastern Cambodia and northern Laos. Additionally, northern Laos and some pockets in Myanmar showed high hotspot intensity, capable of generating a maximum Fire Radiative Power (FRP) >1,000 MW. The return periods for 8, 20, 40, and 120 MW were found to be 0.05, 0.1, 0.5, and 1 year, respectively. In the next 50 years, the entire area will have a 90–100% probability of experiencing up to 40 MW, while central, some parts of northern and southern Myanmar, southern, some parts of northern, central, and northeastern Thailand, and southern Cambodia will have <70% chance of experiencing 120 MW. Hotspots are more frequent at low elevations, on gentle slopes, and across all aspects (excluding flat areas). Moreover, higher elevations, steeper slopes, and southern aspects tend to experience more high-intensity. It can be inferred that fire intensity is not primarily influenced by temperature, precipitation, or relative humidity. Instead, other factors, such as fuel availability and human activities, may play a more significant role.

Keyword: Hotspot, Fire Radiative Power, Frequency-Magnitude Distribution, geographic-meteorological factors

1.Introduction

Air pollution is a critical issue impacting the environment and the quality of life in many countries and has become a significant problem in Southeast Asia (Gu et al., 2024). According to the regional estimates of the World Health Organization (WHO), over 2 million deaths annually in Southeast Asia are attributed to air pollution (Taghizadeh-Hesary & Taghizadeh-Hesary, 2020). This issue arises primarily from emissions caused by wildfires, agricultural burning, biomass burning, transportation, and industrial sources (Miller & Newby, 2020; Moran et al., 2019; Chavanaves et al., 2021), which are key contributors to air pollution. One of the most hazardous pollutants is particulate matter with a diameter of less than 2.5 microns

(PM2.5). This pollutant can enter the respiratory system, deeply penetrate the lungs, and enter the bloodstream, leading to various severe health issues. (Xing, 2016; Li et al., 2018; Chen et al., 2013; Pope et al., 2002). It also impacts the economy, society, environment (Chaiboonsri et al., 2023), and tourism (Yang et al., 2022; Nonthapot et al., 2024). Research by Gu et al. (2024) highlights that the total PM2.5 concentration in Myanmar, Cambodia, Laos, and Thailand was significantly up to twice as high-during the northeast monsoon season.

In the context of studying wildfires, agricultural burning, and biomass burning, Fire Radiative Power (FRP) is a quantitative measure of radiant heat emissions and is recognized as a key indicator for assessing fire intensity (Kumar & Kumar, 2022). It can also be used to calculate fire emissions and environmental impacts. For instance, Vadrevu et al. (2012) studied the relationship between FRP and the types of vegetation burned to determine which areas experience more intense fires. Kaiser et al. (2012) calculated gas and aerosol emissions from biomass burning using the Global Fire Assimilation System (GFASv1.0), which utilizes FRP data. Engel et al. (2022) developed and evaluated a method for calculating FRP for BRIGHT/AHI hotspots to enable real-time fire energy reporting. The FRP value is recorded in hotspots, which are points on the Earth's surface with abnormally high heat values or satellite image pixels with high infrared radiation intensity. These hotspots are often caused by wildfires, agricultural burning, and biomass burning (Korontzi et al., 2006.)

Hotspots can occur from both human-related activities and natural factors, and many studies indicate that human activities are the primary cause of fire occurrences (Ganteaume et al., 2013; Rogers et al., 2020; Sjöström & Granström, 2023). Although hotspots are mainly caused by human activities, topographical and meteorological factors also play a crucial role in determining the distribution and intensity of hotspots. For example, at higher elevations, a significant increase in wildfires has been observed (Kumar & Kumar, 2022). Increased slope steepness affects the spread and intensity of wildfires (Baltaci & Yildirim, 2020). Forest fire occurrence in Central Europe is driven by a combination of human activities and climate conditions. Rising temperatures and decreasing rainfall increase the likelihood of wildfires (Berčák et al., 2024). The rate of wildfire spread is fastest when strong winds, low humidity, and high temperatures coincide. Global and regional climatic factors contribute to variations in wildfire patterns across different regions (Gedalof, 2011). Hotspot are detectable through MODIS (Moderate Resolution Imaging Spectroradiometer), a sensor mounted on NASA's Terra and Aqua satellites, capable of accurately recording hotspot data, covering entire countries, and near real-time data.

To help mitigate the impacts or risks associated with fire, various studies have examined fire prediction using different models as follows: Dorodnykh et al. (2022) researched Forest Fire Risk Forecasting with the Aid of Case-Based Reasoning (CBR) in Irkutsk Oblast, Russia. It was found that CBR model can accurately predict wildfire risk areas. The accuracy score was used to evaluate the wildfire risk forecasting results. The model's accuracy rate is 51%, indicating its potential for further improvement.

According to Kadir et al. (2023) researched the Long Short-Term Memory (LSTM) algorithm, a deep learning method, and wildfire hotspot dataset from MODIS (2010-2022), was applied to analyze and then forecast the number of wildfire hotspots in Indonesia. The forecast for the number of hotspots in 2023 achieved good results with an average error of 7%.

Another study by Nami et al. (2008) predicted wildfire probability in northern Iran's Hyrcanian ecoregion using the Evidential Belief Function (EBF) model. The resulting probability

map showed that moderate to very high-risk zones covered nearly 60% of the landscape, with human infrastructure being a key influencing factor. Validation confirmed the model's effectiveness, showing a prediction rate of 81.03%.

As mentioned above, the purpose of this study was to analyze the hotspot activity and to study the relationship between hotspots and geographic-meteorological factors in Thailand and neighboring countries. The Frequency-Magnitude Distribution (FMD), has been applied in various fields, such as probabilities of Earthquake Occurrences (Pailoplee, 2017), the spatial distribution of rainfall (Prasertwiriya, 2020), tsunami occurrence probability (Olabarrieta et al., 2017), and the frequency distribution of crater sizes (Chorhirankul, 2017; Khamsiri, 2017). In this study, the FMD is integrated with MODIS hotspot data to represent spatial and temporal distributions and to identify relationships with geographic and meteorological factors. This approach aims to assess fire risk in this area, enabling effective hotspot tracking across and supporting timely wildfire management planning.

2. Dataset and Completeness

MODIS hotspot data for the period 2000 to 2022 from NASA FIRMS (Fire Information for Resource Management System) in Figure 1. The datasets contain the geographical locations of fire point centers, each representing a 1×1 km area, along with the date and time of occurrence. The data is organized in the following format: longitude, latitude, year, month, day, FRP (Megawatt: MW), depth, hour, minute, and second, as shown in Table 1.

The 30-meter Digital Elevation Model (DEM) from the website of The United States Geological Survey (USGS) provides elevation data at a spatial resolution of 30 meters, which is useful for topographic analysis, hydrological modeling, and terrain visualization. By using Geographic Information Systems (GIS), the DEM can be processed to derive key topographic features such as elevation, slope, and aspect, which are essential for understanding terrain characteristics

The data is organized and verified as follows: daily mean temperature and precipitation from The National Oceanic and Atmospheric Administration (NOAA), and daily relative humidity from Thai Meteorological Department (TMD) for the period from year 2000 to 2022.

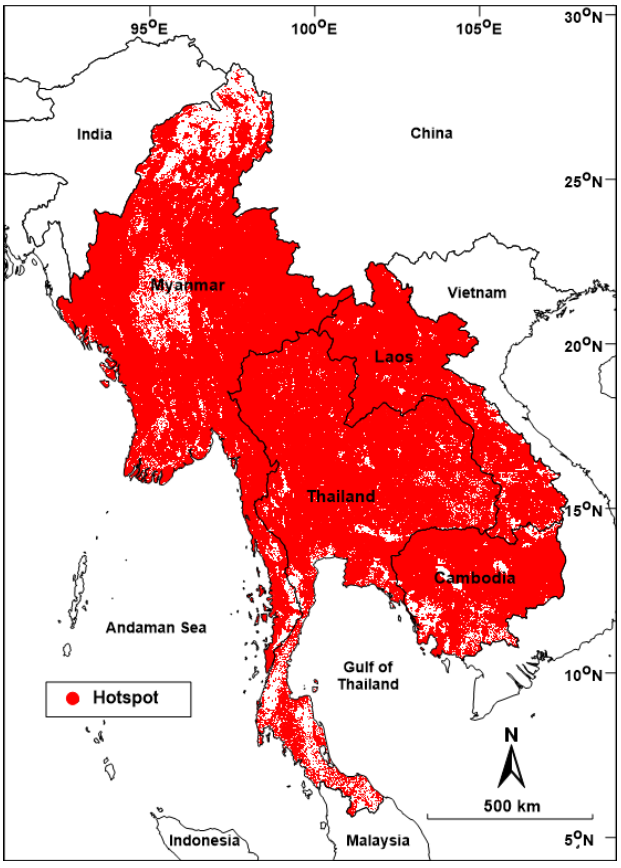

Figure 1 MODIS hotspot data in Thailand and neighboring countries (Myanmar, Laos, and Cambodia) from 2000 to 2022.

Table 1 Example of hotspot data format used for FMD.

Longitude	Latitude	Year	Month	Day	FRP	Depth	Hour	Min	Second
102.00	14.12	2000	11	1	5.5	0	15	54	0
101.95	14.13	2000	11	1	5.0	0	15	54	0
99.37	22.86	2000	11	2	11.4	0	4	6	0
103.13	19.40	2000	11	2	3.9	0	4	7	0
105.14	17.44	2000	11	2	8.7	0	4	7	0
105.15	17.44	2000	11	2	7.4	0	4	7	0

3. Hotspot activity

3.1 Frequency-FRP

Ishimoto and Iida (1939) and Gutenberg and Richter (1944) presented Frequency-Magnitude Distribution (FMD), which represents the relationship indicating the number or rate of occurrences of events across different times and areas, as explained by the Equation (1);

$$\log(N_M) = a - bM \text{ or } \ln(N) = ln\alpha - \beta M \quad (1)$$

Where N_M is the cumulative number of hotspots with a FRP equal to or greater than M. Both a and b are positive constants that vary across different times and specific areas. The a value represents the total number or rate of occurrence of events of all sizes while b value represents the ratio of larger events to smaller ones. The value of α and β are constants related to a and b as expressed by Equation (2) and (3), respectively;

$$\alpha = \exp(a \ln(10)) \quad (2)$$

and

$$\beta = bln(10) \quad (3)$$

The research area was gridded at 0.25° x 0.25° spacing to analyze hotspot activity. Using MODIS hotspot data for the period 2000 to 2022 from NASA FIRMS MODIS (3,332,121 hotspots), those within an empirically fixed 25 km radius of each grid node were selected and contributed to the FMD. The a-value, b-value, percent of goodness fit, and megawatt of completeness (mc-value) were then computed and spatially mapped using the ZMAP tool (Wiemer, 2001). Finally, the obtained values were then contoured and mapped, as illustrated in Figure 2.

The spatial distribution of the a-values was all in the range of 1.4–4.4 (Figure 2a). Areas with high a-values (>4), indicating high hotspot activity, were primarily observed at (i) northwestern to eastern Cambodia, and (ii) northern Laos. In contrast, areas with low a-values (<2), indicating low hotspot activity, were observed at (i) southern Thailand and (ii) central Myanmar.

The spatial distribution of the b-values was all in the range of 0-0.05 (Figure 2b). Areas with high b-values (>0.04), indicating low intensity, were observed at (i) central Myanmar, (ii) southern Myanmar, (iii) and central to lower northern Thailand, (iv) and southern Thailand. In contrast, areas with low b-values (<0.005), indicating high intensity, were primarily observed at northern Laos.

The spatial distribution of the mc-values was all in the range of 5–10 (Figure 2c). Almost the area showing low mc-value (5), while there are some scattered pockets with high mc-values.

In addition, the goodness of fit (Figure 2d) computing the difference between the observed FMD and hotspot distribution, the lower difference showing the higher goodness of fit.

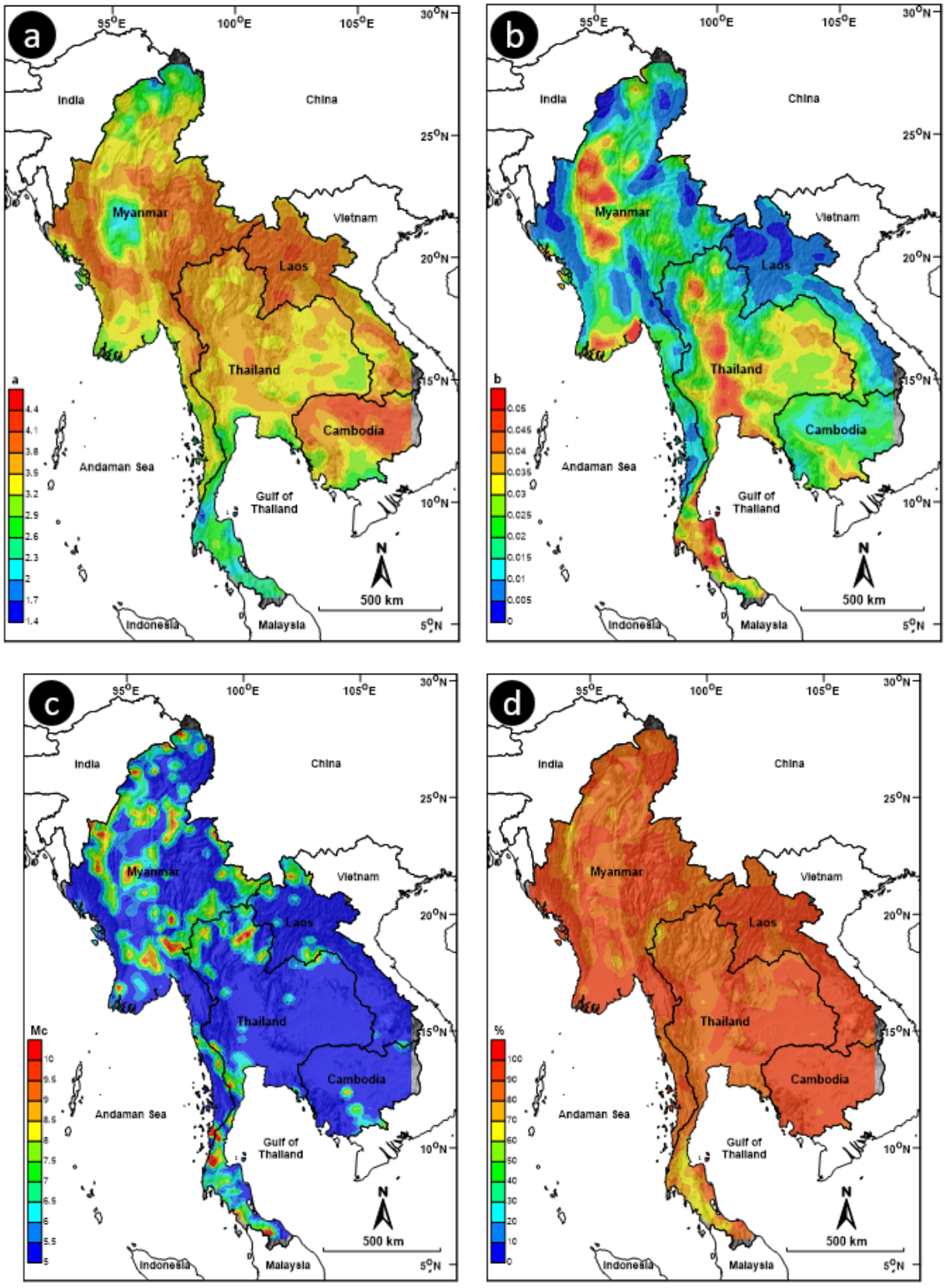

Figure 2 Spatial distributions of the (a) *a*-value, (b) *b*-value, (c) mc-value, and (e) the goodness fit of the FMD.

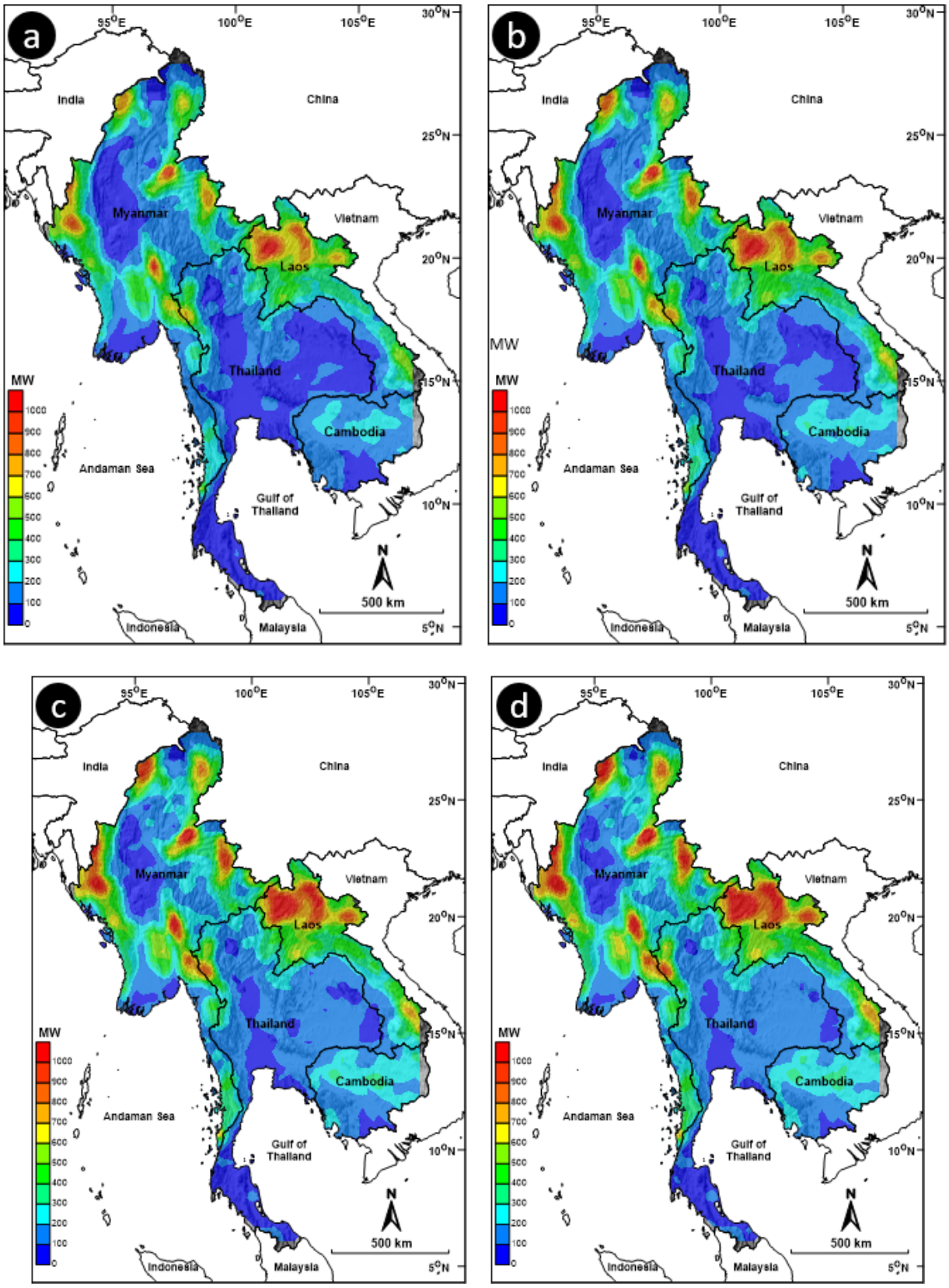

Figure 3 The probable maximum FRP value of hotspot capable of being generated in the individual time span of the next (a) 5, (b) 10, (c) 30, and (d) 50 years.

3.2 Most probable maximum FRP

Yadav et al. (2011), applied the α and β values the FMD equation to assess earthquake occurrence behaviors in various forms. In this study, we use them to estimate the most probable maximum FRP over a period of t years of interest (u_t) as expressed in Equation (4).

$$u_t = \frac{\ln(\alpha t)}{\beta} \quad (4)$$

Where u_t (MW) is the most probable maximum FRP in the period of t.

The most probable maximum FRP value of hotspot that could be generated in 5, 10, 30 and 50 years was then calculated and mapped, as illustrated in Figure 3. The probable maximum FRP value of hotspot capable of being generated in the next 5 and 10 years (Figure 3a, 3b), showing similar results. Areas with high FRP value (>600 MW), were observed at (i) northern Laos and (ii) some pockets in Myanmar. Meanwhile, most area are low FRP value (<200 MW), especially in Thailand and central Myanmar, where the FRP values are very low (<100 MW).

The probable maximum FRP value of hotspot capable of being generated in the next 30 and 50 years (Figure 3c, 3d), showing similar results. Areas with high FRP value (>600 MW) have increased and expanded, primarily observed at (i) northern Laos and some pockets (ii) in Myanmar. Meanwhile, areas with low FRP value (<200 MW) have decreased, especially in Thailand, where areas with very low FRP values (<100 MW) have significantly decreased.

The results of the maximum FRP indicate that the very high-intensity zone is located in northern Laos and some pockets in Myanmar. In contrast, the very low-intensity zone spans from central to southern Thailand and central Myanmar.

3.3 Hotspot return period

Return period is calculated by α and β values as expressed in Equation (5) (Yadav et al., 2011).

$$T_M = \frac{\exp(\beta M)}{\alpha} \quad (5)$$

Where T_M (year) is the expected time interval for the occurrence of a hotspot with FRP greater than or equal to M.

FRP values are selected from occurrence statistics within 23 years (2000-2022) as 8, 20, 40, and 120 MW for determining the return periods in Figure 4.

Return period of hotspot with FRP value 8 MW was all in the range of 0–0.5 year (Figure 4a). The results reveal that almost all area have a return period of 8 MW in 0.05 year (18 days). Southern Thailand and northern Myanmar have a return period ≥ 0.15 year (55 days). Central Myanmar has a return period ≥ 0.2 year (73 days).

Return period of hotspot with FRP value 20 MW was all in the range of 0–1 year (Figure 4b). The results reveal that almost all area have a return period of 20 MW in 0.1 year (37 days). Southern Thailand and northern part of Myanmar have a return period ≥ 0.3 year (110 days). Central Myanmar has a return period ≥ 0.4 year (146 days).

Return period of hotspot with FRP value 40 MW was all in the range of 0–5 years (Figure 4c). The results reveal that almost all area have a return period of 40 MW in 0.5 year (183 days). Meanwhile, the southern Thailand, northern, central, and some parts of southern Myanmar have a return period ≥ 2 years.

Return period of hotspot with FRP value 120 MW was all in the range of 0–10 years (Figure 4d). The results reveal that Laos, almost all of Cambodia, some parts of Myanmar, and the border areas in northern Thailand have a return period of 120 MW in 1 year. Meanwhile,

almost all Thailand, northern, central, some parts of southern Myanmar and southern Cambodia have a return period ≥ 10 years.

3.4 Probability of hotspot occurrence

The probabilities of occurrences, $P_t(M)$, for any given specific time period (t) and certain FRP (MW) were also evaluated as expressed in Equation (6)

$$P_t(M) = 1 - \exp\left(-\alpha t(\exp(-\beta M))\right) \quad (6)$$

Where P_t (%) is probabilities of occurrences, M, in '*0*' year

The probability of hotspot occurrence with FRP value 8, 20, 40, 120 MW in the next 50 years as show in Figure 5.

The probability of hotspot occurrence with FRP value 8 MW in the next 50 years (Figure 5a) is 100% for all areas. The probability of hotspot occurrence with FRP value 20 MW in the next 50 years (Figure 5b) is between 99% and 100% for all areas. The probability of hotspot occurrence with FRP value 40 MW in the next 50 years (Figure 5c) is almost 100% in all areas, except for some area at the southern coast of Thailand, which is 40%. Finally, the probability of hotspot occurrence with an FRP value of 120 MW in the next 50 years is shown in Figure 5d. The results reveal that Laos, almost all of Cambodia and Myanmar, and some parts of northern, central, and northeastern Thailand have a 100% probability. Meanwhile, the probability of occurrence is less than 70% for central, some parts of northern and southern Myanmar, southern, some parts of northern, central, and northeastern Thailand, and southern Cambodia.

4. Relationship with geography factors

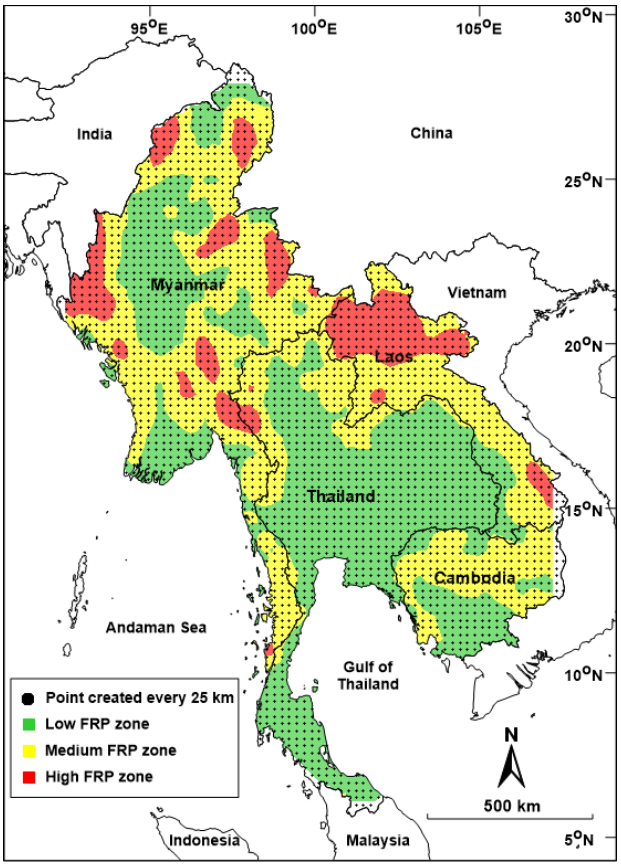

Figure 6 Points created every 25 km.

In this part, the study focuses on the relationship between hotspots and geographical factors. Specifically, it examines (i) elevation, (ii) slope, and (iii) aspect, which are represented at points created every 25 km in Figure 6. Then, these factors overlay with the map of the probable maximum FRP values of hotspots capable of being generated in the next 50 years (Figure 3d). The zones are categorized by the intensity of FRP values as follows: (i) low (<200 MW), (ii) medium (200-600 MW), and (iii) high (>600 MW), as illustrated in Figure 7–9. Furthermore, illustrative examples of elevation, slope, and aspect levels in each zone are also provided in Figure 10–12.

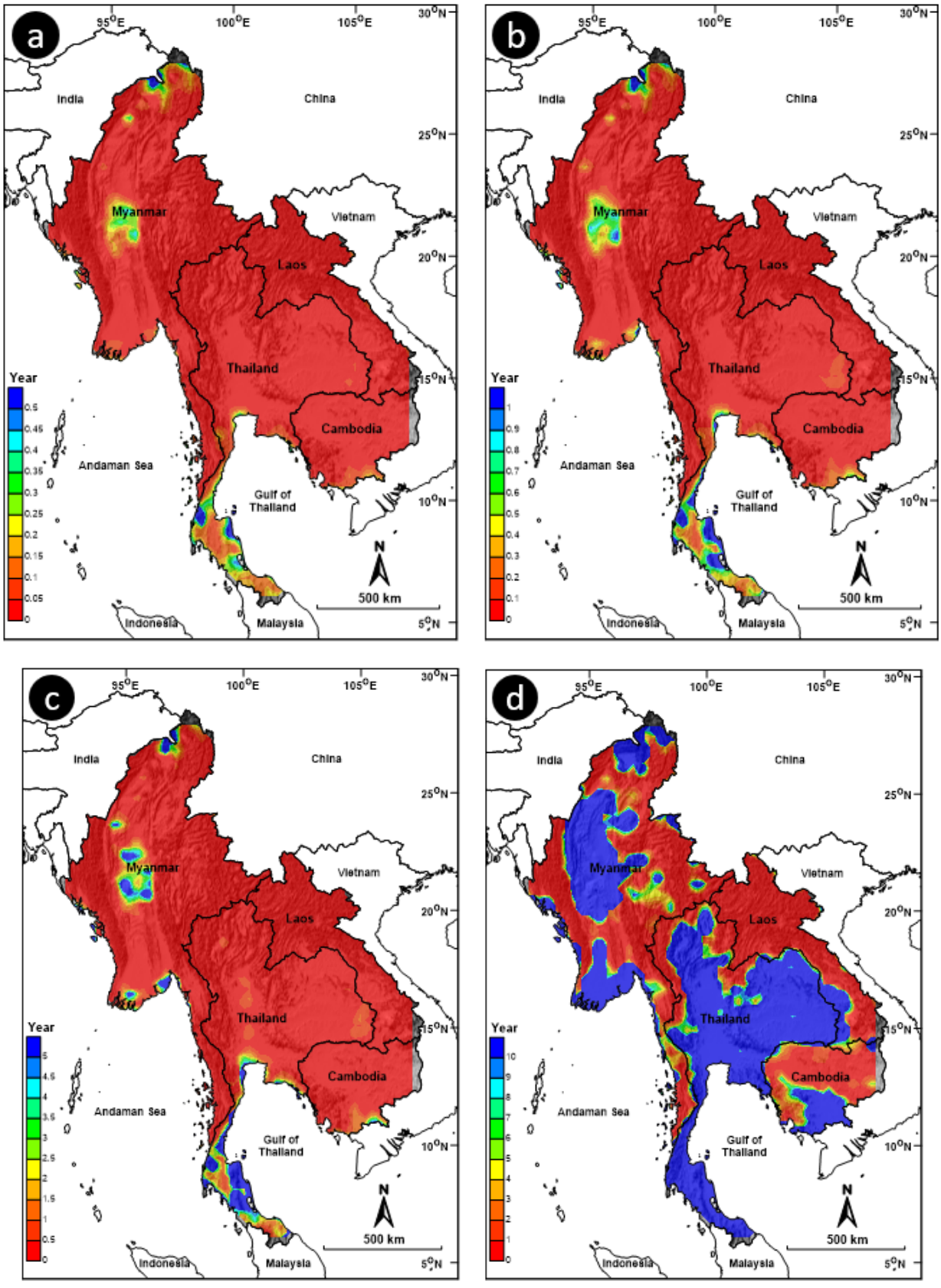

Figure 4 Return periods of hotspot with FRP value (a) 8, (b) 20, (c) 40, and (d) 120 MW.

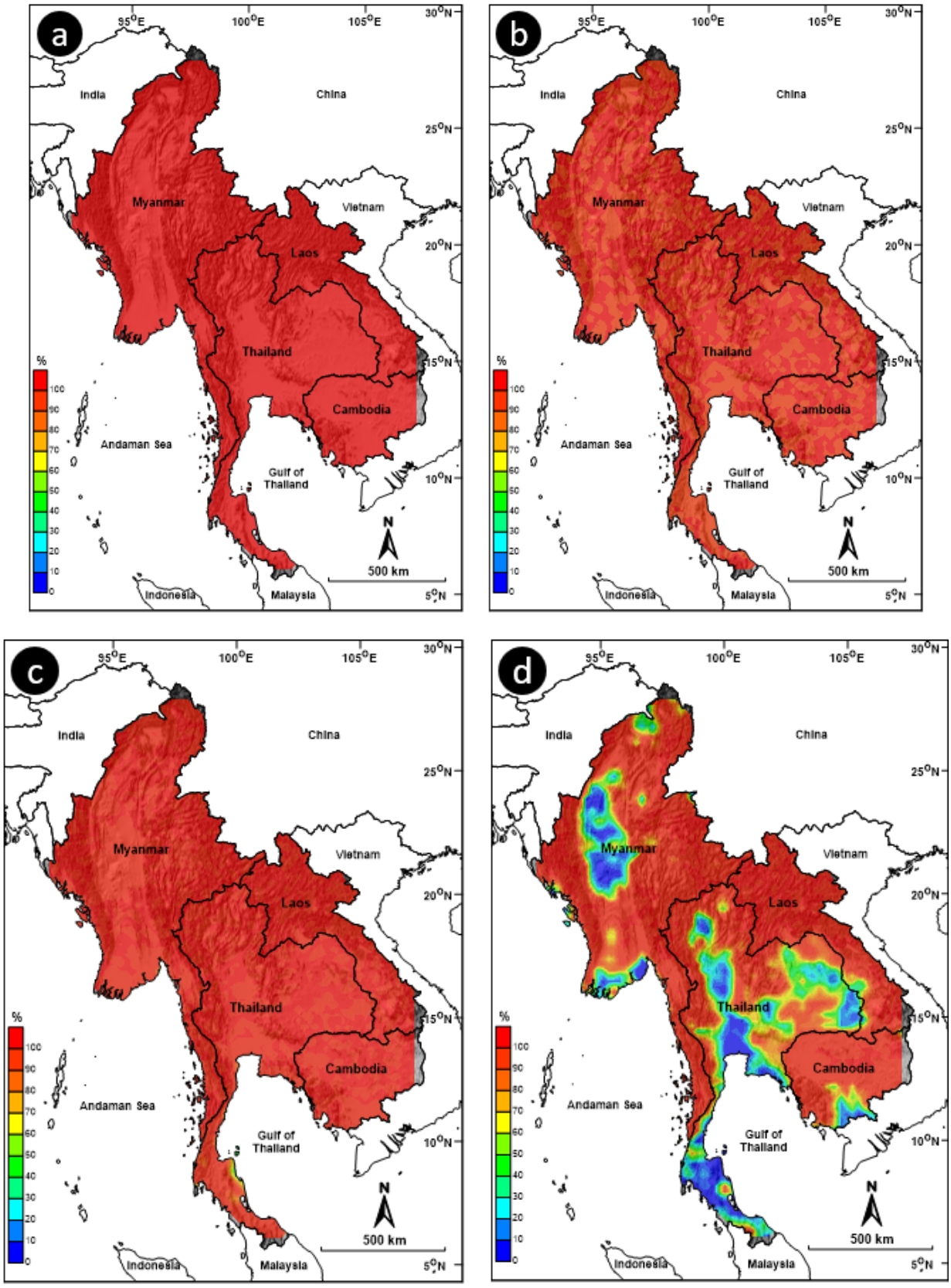

Figure 5 Probability of hotspots occurrence with FRP value (a) 8, (b) 20, (c) 40, and (d) 120 MW in the next 50 years.

4.1 Elevation

Figure 7 illustrates the distribution of points based on three elevation ranges: 0–499 m, 500–1000 m, and more than 1,000 m and three zones of FRP intensity: low, medium, and high. This allows for a clear visualization of how points are distributed based on both elevation and the intensity of FRP values.

Most points are located at lower elevations (0–499 m), with a total of 1,741 points. Among these, the majority (1,019 points) are classified as belonging to the low zone, followed by 617 points in the medium zone, and 75 points in the high zone.

In the 500–1000 m elevation range, there are 533 points. The distribution changes here, with 289 points falling into the medium zone, 144 points in the high zone, and only 100 points in the low zone.

For elevations above 1,000 m, there are 355 points. The medium zone again has the highest number of points (195), while 98 points are in the high zone, and 62 points are in the low zone.

Based on the analysis, it is evident that the distribution of points and their associated zone levels varies with elevation. Most points are located at lower elevations (0–499 m), the majority of points are classified as low FRP zone. However, as elevation increases, the proportion of points with medium and high FRP zone also increases. In the 500-1000 m range, medium FRP zone becomes more prevalent, while at elevations above 1000 m, medium FRP zone remains the most common, but high FRP zone is also significantly present.

4.2 Slope

Figure 8 illustrates the distribution of points based on five slope ranges: flat to gentle (0–3%), moderate (3–12%), steep (12–20%), very steep (20–35%), and extreme (>35%) from UNEP/FAO (Iaaich et al., 2016) and three zones of FRP intensity: low, medium, and high.

In the 0-3% slope range, there are 366 points with low zone, 166 medium zone points, and 6 high zone points. In the 3-12% slope range has the highest number of points, the majority of points (555) are classified as low zone, followed by 330 points with medium zone, and 37 points with high zone. In the 12-20% slope range, there are 131 points with medium zone, 73 points with low zone, and 39 points with high zone. In the20-35% slope range, there are 204 points with medium zone, 98 points with low zone, and 83 points with high zone. In the slope range greater than 35%, there are 270 points with medium zone, 119 points with low zone, and 152 points with high zone.

Based on the analysis, it is evident that the distribution of points and their associated zone levels varies with slope. The majority of points within the 3–12% slope range, in 0–12% slope range show low FRP zone. In contrast, the high FRP zone is predominantly found in more than 20% slope, especially beyond 35%. This indicates a possible correlation between slope steepness and fire risk or intensity.

4.3 Aspect

Figure 9 illustrates the distribution of points based on nine aspect ranges: Flat, North (N), Northeast (NE), East (E), Southeast (SE), South (S), Southwest (SW), West (W), Northwest (NW) and three zones of FRP intensity: low, medium, and high.

In the Flat area, there are the fewest points, with only 56 points in total and none in the high zone. Meanwhile, in the North facing slopes, there are the most points, with 164 points in the low zone, 150 in the medium zone, and 38 in the high zone. The Northeast facing slopes has 150 points with low zone, 120 with medium zone, and 37 with high zone. In the East facing slopes, there are 148 points with low zone, 137 with medium zone, and 37 with high zone. The Southeast facing slopes has 163 points with low zone, 144 with medium zone, and 36 with high

zone. In the South facing slopes, there are 137 points with low zone, 142 with medium zone, and 44 with high zone. For the Southwest facing slopes, there are 119 points with low zone, 124 with medium zone, and 45 with high zone. The West facing slopes has 156 points with low zone, 130 with medium zone, and 43 with high zone. Lastly, the Northwest facing slopes has 143 points with low zone, 129 with medium zone, and 37 with high zone.

Based on the analysis, it is evident that the distribution of points and their associated zone levels varies with aspects. The Flat facing slopes exhibits the lowest number of points, with no high FRP zone point, indicating a relatively safer terrain. In contrast, the North facing slopes observes the most points, followed sequentially by the Southeast, West, South, East, Northwest, Northeast, and Southwest. However, the South, Southwest, and West facing slopes show a notable increase in high FRP zone points.

5. Relationship with Meteorology factors

This part focuses on the relationship between hotspots and meteorological factors. Specifically, it examines (i) temperature, (ii) precipitation from NOAA, and (iii) relative humidity from TMD, with the locations of the meteorological stations shown in Figure 13. These factors were analyzed in conjunction with the FRP values of hotspots occurring in each zone (low, medium, and high zones). The analysis uses FRP data from hotspots within

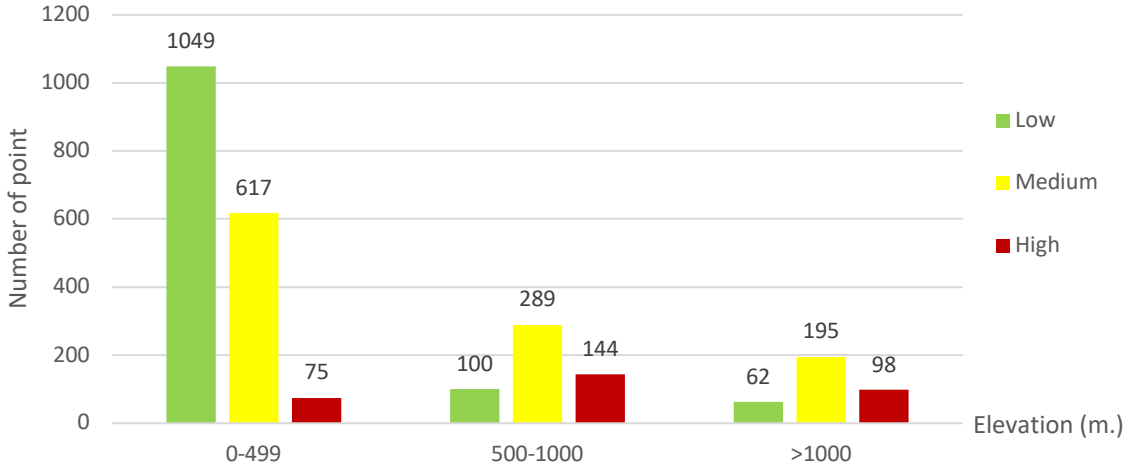

Figure 7 Distribution of points by elevation with FRP intensity zones.

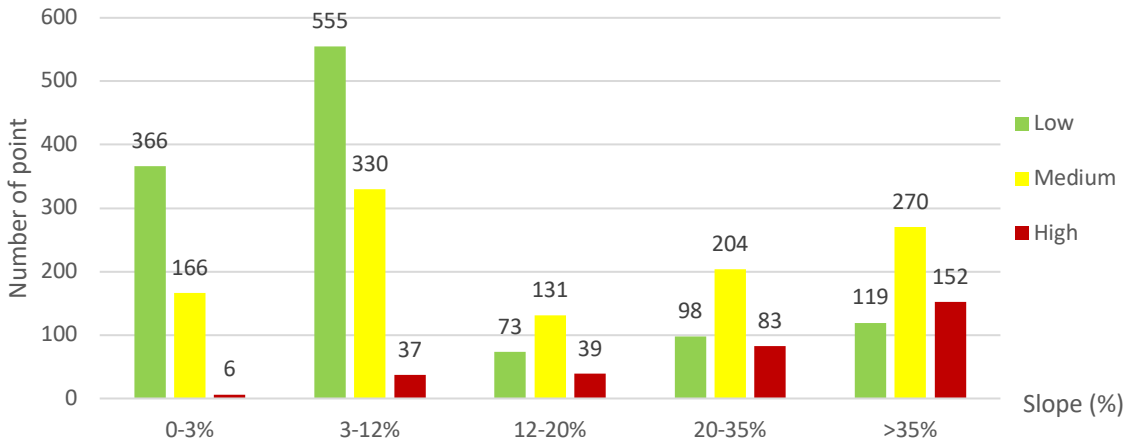

Figure 8 Distribution of points by slope with FRP intensity zones.

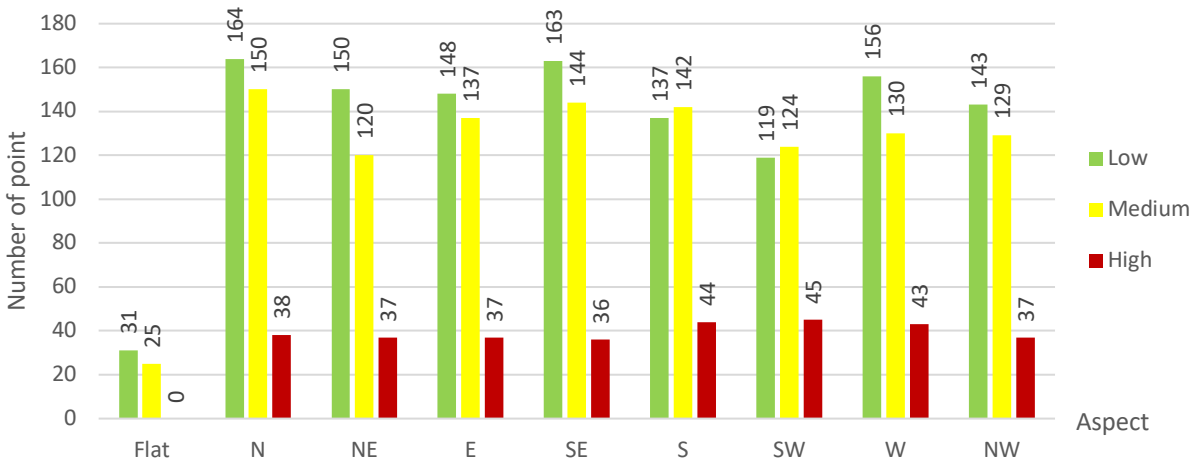

Figure 9 Distribution of points by aspect with FRP intensity zones.

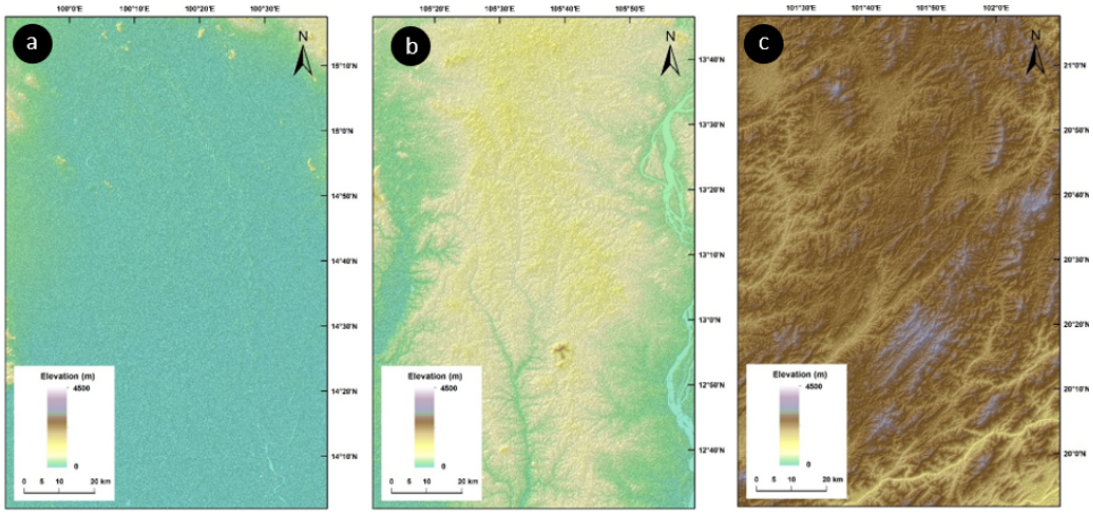

Figure 10 Examples of elevation in (a) low, (b) medium, and (c) high zone.

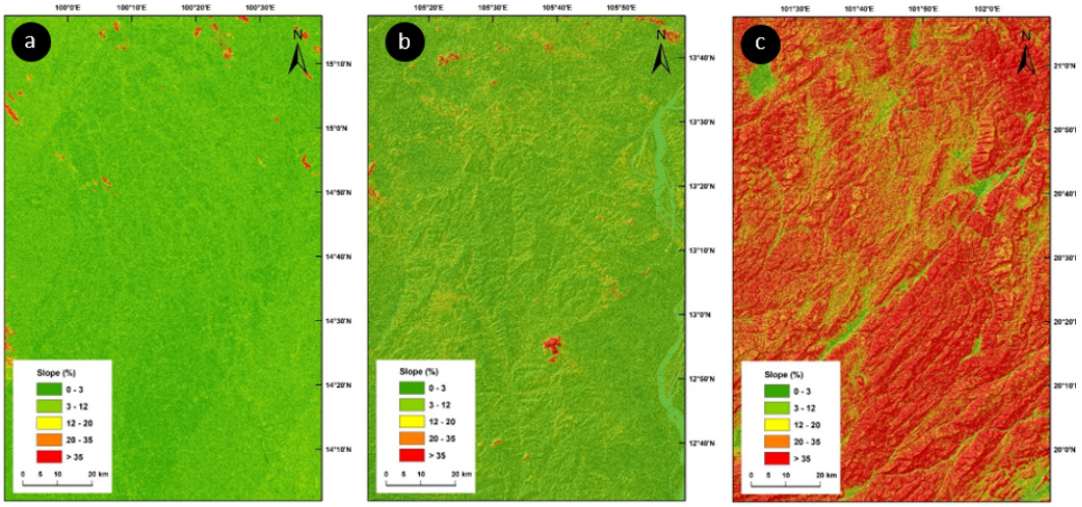

Figure 11 Examples of slope in (a) low, (b) medium, and (c) high zone.

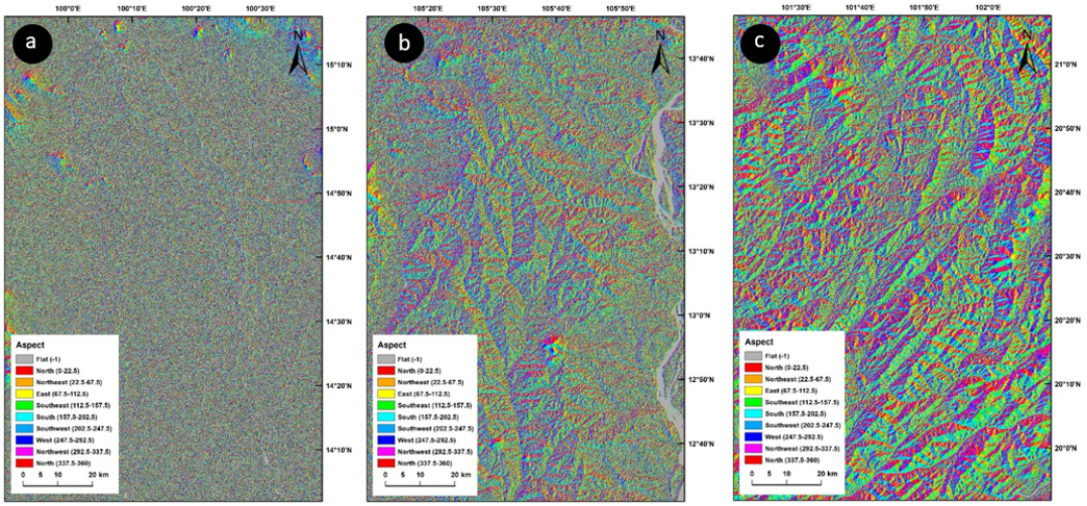

Figure 12 Examples of aspect in (a) low, (b) medium, and (c) high zone.

a 25 km radius around meteorological stations, with daily comparisons presented from 2000 to 2022, as illustrated in Figure 14–16.

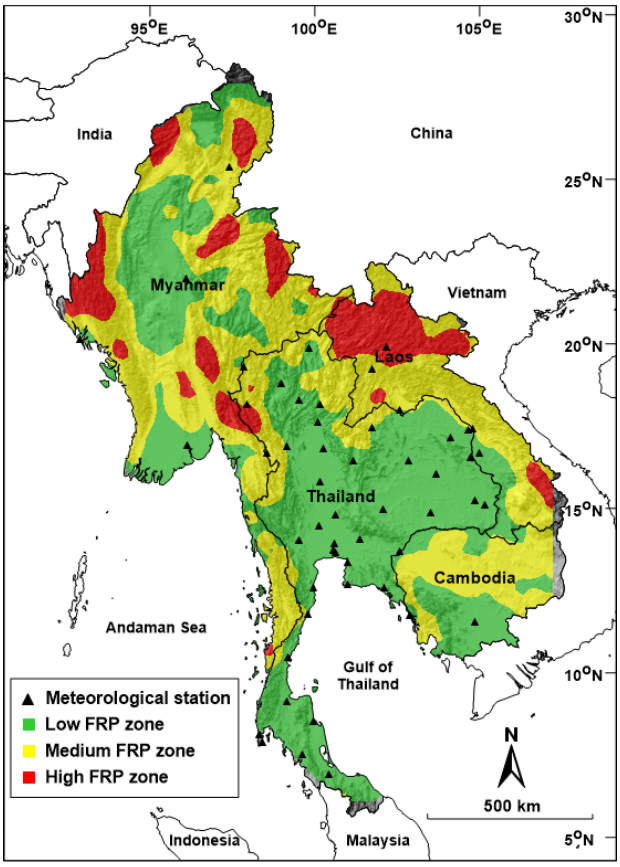

Figure 13 Locations of meteorological stations.

5.1 Low FRP zone

By selecting meteorological data from the Lopburi meteorological station in Thailand and FRP data from hotspots within a 25 km radius around the station as a representative for the analysis of the low FRP zone, the results are as follows and are presented in Figure 14.

The pattern of mean FRP in the low FRP zone (Figure 14a). The values fluctuate, showing a cyclical pattern. These peaks occur regularly each year, indicating occasional fire activity, with the highest value occurring near 150 MW at the end of 2019, possibly due to external environmental factors.

The pattern of temperature in low FRP zone (Figure 14b). Seasonal variations are noticeable, with regular cyclical patterns. There is no extreme long-term increase or decrease, but periodic short-term fluctuations.

The pattern of precipitation in low FRP zone (Figure 14c). The distribution is highly variable, with frequent occurrences of rainfall events ranging from minimal amounts to over 90 mm (very heavy rain) in certain instances. Increased precipitation might help suppress fire activity.

The pattern of relative humidity in low FRP zone (Figure 14d). The values fluctuate seasonally, showing a cyclical pattern that follows typical atmospheric moisture variations. High humidity levels likely contribute to reducing fire activity.

Overall, the findings suggest that fire activity in the low FRP zone shows high FRP values each year that are quite similar. These activities are regulated by natural climatic variations. High humidity and frequent rainfall events appear to limit fire intensity and spread.

5.2 Medium FRP zone

By selecting meteorological data from the Loei meteorological station in Thailand and FRP data from hotspots within a 25 km radius around the station as a representative for the analysis of the medium FRP zone, the results are as follows and are presented in Figure 15.

The pattern of mean FRP in the medium FRP zone (Figure 15a) illustrates the variation over time. There is a high value in the early period, with the highest value occurring over 200 MW at the end of 2005. A general decreasing trend in FRP is noticeable over time, particularly after around 2010, where the magnitude and frequency of peak FRP events appear to decline.

The pattern of temperature in medium FRP zone (Figure 15b) represents the fluctuations in temperature across the years. A clear seasonal cycle is evident, with periodic increases and decreases indicating annual

temperature variations. The temperature appears relatively stable over the years.

The pattern of precipitation in medium FRP zone (Figure 15c) shows a sporadic pattern with peaks occurring at different times. After 2010, rainfall intensity increases several years.

The pattern of relative humidity in medium FRP zone (Figure 15d), which follows a distinct seasonal pattern similar to that of temperature. The data show that relative humidity fluctuates cyclically over time, with values mostly ranging between 40% and 95%, indicating consistent atmospheric moisture levels.

Overall, this analysis illustrates that FRP has shown a decreasing trend over the years, particularly after 2010. Temperature and relative humidity exhibit stable seasonal cycles without any significant long-term trends. Rainfall, although highly variable, does not display a clear increasing or decreasing pattern. These findings suggest that fire activity (as indicated by FRP) may be declining, potentially influenced by climatic conditions such as temperature, rainfall, and humidity

5.3 High FRP zone

By selecting meteorological data from the Mae Hong Son meteorological station in Thailand and FRP data from hotspots within a 25 km radius around the station as a representative for the analysis of the high FRP zone, the results are as follows and are presented in Figure 16.

The pattern of mean FRP in the high FRP zone (Figure 16a). There are several peaks in the graph, indicating periods of higher fire activity, with the highest value occurring near 500 MW in 2010. After that, the trend shows a decreasing pattern.

The pattern of Temperature in high FRP zone (Figure 16b) Over the years, there is no significant long-term increasing or decreasing trend, and the values remain relatively stable, following a consistent periodic pattern.

The pattern of precipitation in high FRP zone (Figure 16c). Rainfall events appear sporadic, with peaks occurring at different points across the years. Although the rainfall pattern is highly variable, an increase in peak rainfall amounts can be observed around the 2004–2006.

The pattern of relative humidity in high FRP zone (Figure 16d), reveals a seasonal pattern, fluctuating between approximately 40% and 100%. The cyclical nature of the data suggests regular changes in humidity levels throughout the years.

Overall, the pattern of FRP and climatic factors in a high FRP zone reveal that FRP was significantly higher in the early years but has shown a decreasing trend since around 2011, with fewer extreme fire events occurring in recent years. Temperature and relative humidity follow stable seasonal cycles without any long-term trends. Although rainfall is variable, it exhibits some peaks during 2004–2006, without showing a clear increasing or decreasing trend. These observations suggest that while fire activity (as indicated by FRP) has decreased over time, the climatic factors such as temperature, rainfall, and humidity have remained relatively stable.

6. Discussions and Conclusion

In this study, we focused on the analysis of hotspots in Thailand and nearby countries. The spatial variations in *a*- and *b*-values derived from the Frequency-Magnitude Distribution (FMD) were studied and visualized through mapping. Furthermore, parameters associated with the hotspots were assessed utilizing the calculated *a*- and *b*-values.

For the most probable maximum FRP in 5, 10, 30, 50 years, they indicate that very high-intensity zones are located in northern Laos and

some pockets in Myanmar, with the highest FRP values exceeding 1,000 MW. Satellite imagery from Google Earth reveals that these areas consist of forests and shrubland/savanna, which have high biomass resulting in elevated FRP value,

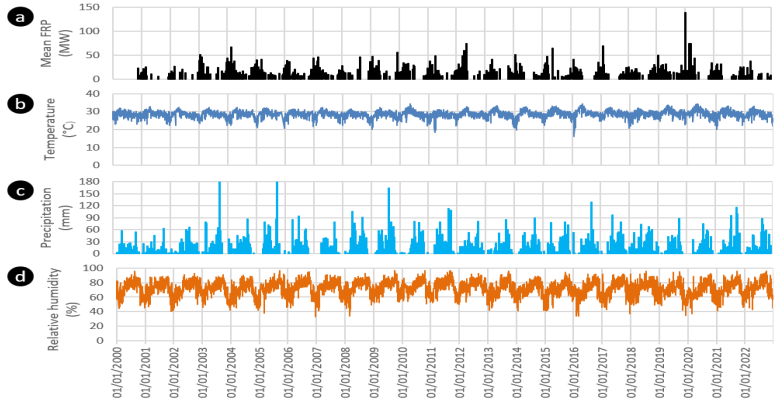

Figure 14 The pattern of (a) mean FRP, (b) temperature, (c) rainfall, and (d) relative humidity from 2000–2022 in low FRP zone.

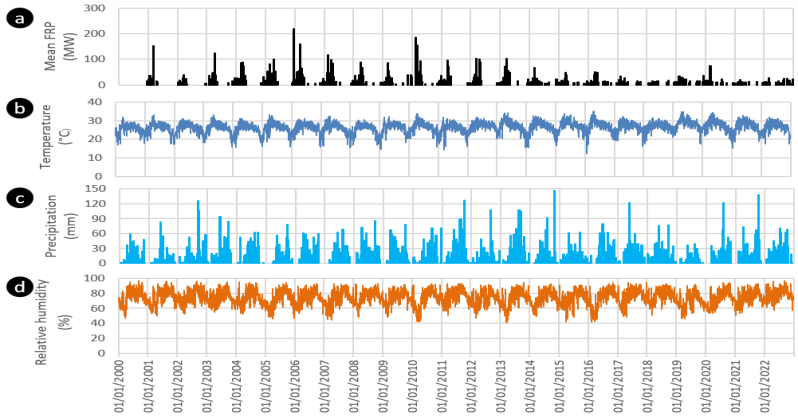

Figure 15 The pattern of (a) mean FRP, (b) temperature, (c) rainfall, and (d) relative humidity from 2000–2022 in medium FRP zone.

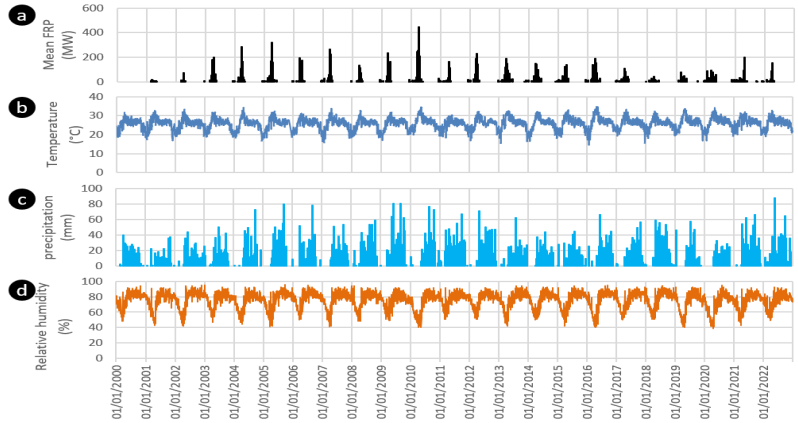

Figure 16 The pattern of (a) mean FRP, (b) temperature, (c) rainfall, and (d) relative humidity from 2000–2022 in high FRP zone.

similar to the land cover classes (MCD12Q1) from MODIS in the study by Adaktylou (2024). Conversely, the very low-intensity zones are found from central to southern Thailand and central Myanmar, where these areas are primarily croplands.

The recurrence maps reveal the diversity of recurrence intervals across Thailand and neighboring countries. Most regions exhibit short periods of recurrence (0.05, 0.1, 0.5, and 1 year) at FRP of 8, 20, 40, and 120 MW, respectively. However, almost all areas within Thailand, along with northern, central, and southern Myanmar, as well as southern Cambodia, experience longer recurrence periods specifically at 120 MW.

The probability of hotspot occurrence in the next 50 years, almost all areas will have 100% probability for every FRP value, except central, some parts of northern and southern Myanmar, southern, some parts of northern, central, and northeastern Thailand, and southern Cambodia, which have <70% probability at 120 MW. Hotspots in these areas have low FRP values, as these regions are primarily croplands. Agricultural burning practices are typically controlled, with fires confined to specific areas.

There has also been a study on the relationship between hotspots and geography-meteorology factors. It was found that most fire occurrences are concentrated at 0-499 m, with the majority classified as low-intensity fires, possibly because they are often caused by human activities, such as agricultural burning. These occurrences decrease as elevation increases, aligning with the findings of Nami et al. (2008), which indicated that the likelihood of fires diminishes with higher elevations. However, in higher elevation tend to be more severe due to the abundance of natural resources and the availability of highly flammable dry fuels, such as dried leaves and plant debris. These factors contribute to the intensity of the fires, making them capable of spreading rapidly and expanding over larger areas.

Hotspots are more frequent in areas with gentle slopes (0–3% and 3–12%), with low-intensity fires being the most common. However, as the slope increases (>20%), the proportion of medium- and high-intensity fires rises, suggesting that steeper slopes exhibit greater intensity due to key factors like accumulated fuel loads or wind effects, which contribute to fire spread, which is consistent with previous research of Baltaci and Yildirim (2020) which stated that slope is a factor that positively impacts the spread and intensity of fires.

Hotspot distribution appears relatively uniform across all directions, except for flat aspects, where the majority of fires are of low- and medium-intensity. However, a noticeable increase in high-intensity fires is observed in the south, southwest, and west aspects. This aligns with the findings of Pacaldo et al. (2025), who reported that south-facing slopes tend to experience more severe fires due to factors such as higher solar energy absorption, elevated temperatures, strong winds, low humidity, and low fuel moisture (Adab et al., 2013).

In terms of meteorological factors (temperature, precipitation, and relative humidity), they reveal the recurring periods of hotspot occurrences in the same timeframe each year. Although their influence varies among zones, it is generally weak. Rising temperatures have no significant effect on FRP. Most hotspots tend to occur during periods without rainfall, and the intensity of fires ranges from low to high. However, a negative correlation is observed between relative humidity and FRP, suggesting that higher humidity levels tend to reduce fire intensity, likely due to increased moisture in vegetation and reduced flammability. Nonetheless, the weak correlation indicates that while humidity plays a role, it is not the sole determining factor of fire intensity. Instead,

other factors, such as fuel availability or human activities, may have a more significant impact (Ganteaume et al., 2013; Rogers et al., 2020; Sjöström & Granström, 2023).

We found that hotspots typically occur during the dry season, which corresponds with the period of agricultural burning. They are most frequently detected around midday. Areas with high hotspot density are commonly found in agricultural lands or forested areas that have been encroached upon. These findings support the conclusion that human activities are the primary drivers of hotspot occurrences.

Acknowledgement

The authors acknowledge the contributions of all individuals and resources that have provided inspiration and knowledge for this project. Furthermore, we extend our appreciation to the editor and anonymous reviewers for their careful review and insightful recommendations, which have significantly improved this work.

References

Adab, H., Kanniah, K. D., & Solaimani, K. (2013). Modeling forest fire risk in the northeast of Iran using remote sensing and GIS techniques. *Natural hazards*, *65*, 1723-1743. https://doi.org/10.1007/s11069-012-0450-8

Adaktylou, N., Stratoulias, D., Borgman, J., Cha, S., Adiningrat, D. P., & Nuthammachot, N. (2024). Land Cover Disaggregated Fire Occurrence and Particulate Matter 2.5 Relationship in the Mekong Region: A Comprehensive Study. *ISPRS International Journal of Geo-Information, 13*(6), 206. https://doi.org/10.3390/ijgi13060206

Baltaci, U., & Yildirim, F. (2020). Effect of slope on the analysis of forest fire risk. *Hacettepe Journal of Biology and Chemistry, 48*(4), 373-379. https://doi.org/10.15671/hjbc.753080

Berčák, R., Holuša, J., Trombik, J., Resnerová, K., & Hlásny, T. (2024). A combination of human activity and climate drives forest fire occurrence in central europe: the case of the Czech Republic. *Fire, 7*(4), 109. https://doi.org/10.3390/fire7040109

Chaiboonsri, C., Eakkapun, P., Sirimongkonlertkun, N., Suksaroj, T. T., Nasanit, R., Apiratikul, R., Apirakkittikul, N., Manason, P., Wongwuthikun, K., & Pongpiachan, S. (2023). The Impact of PM2.5 on Socio-Economic of Thailand: The Perception Based on The Survey Data. *NIDA Development Journal, 63*(2), 106-124. https://doi.org/10.14456/ndj.2023.5

Chavanaves, S., Fantke, P., Limpaseni, W., Attavanich, W., Panyametheekul, S., Gheewala, S. H., & Prapaspongsa, T. (2021). Health impacts and costs of fine particulate matter formation from road transport in Bangkok Metropolitan Region. *Atmospheric Pollution Research, 12*(10), 101191. https://doi.org/10.1016/j.apr.2021.101191

Chen, H., Burnett, R. T., Kwong, J. C., Villeneuve, P. J., Goldberg, M. S., Brook, R. D., van Donkelaar, A., Jerrett, M., Martin, R.V., Brook, J.R., & Copes, R. (2013). Risk of incident diabetes in relation to long-term exposure to fine particulate matter in Ontario, Canada. *Environmental health perspectives, 121*(7), 804-810. https://doi.org/10.1289/ehp.1205958

Chorhirankul, N. (2017). *Frequency-size distribution of the craters on Mars* [Master's thesis, Chulalongkorn University]. Chulalongkorn University Intellectual Repository. https://cuir.car.chula.ac.th/handle/123456789/61680

Dorodnykh, N., Nikolaychuk, O., Pestova, J., & Yurin, A. (2022). Forest Fire Risk Forecasting with the Aid of Case-Based Reasoning. *Applied Sciences, 12*(17), 8761. https://doi.org/10.3390/app12178761

Engel, C. B., Jones, S. D., & Reinke, K. J. (2022). Fire Radiative Power (FRP) Values for Biogeographical Region and Individual Geostationary HHMMSS Threshold (BRIGHT) Hotspots Derived from the Advanced Himawari Imager (AHI). *Remote Sensing, 14*(11), 2540. https://doi.org/10.3390/rs14112540

Ganteaume, A., Camia, A., Jappiot, M., San-Miguel-Ayanz, J., Long-Fournel, M., & Lampin, C. (2013). A review of the main driving factors of forest fire ignition over Europe. *Environmental management, 51*, 651-662. https://doi.org/10.1007/s00267-012-9961-z

Gedalof, Z. E. (2010). Climate and spatial patterns of wildfire in North America. *The landscape ecology of fire,* 89-115. Dordrecht: Springer Netherlands. https://doi.org/10.1007/978-94-007-0301-8_4.

Gu, Y., Fang, T., & Yim, S. H. L. (2024). Source emission contributions to particulate matter and ozone, and their health impacts in Southeast Asia. *Environment international*, *186,* 108578. https://doi.org/10.1016/j.envint.2024.108578

Gutenberg, B., & Richter, C. F. (1944). Frequency of earthquakes in California. *Bulletin of the Seismological society of America, 34*(4), 185-188. https://doi.org/10.1785/BSSA0340040185

Iaaich, H., Moussadek, R., Baghdad, B., Mrabet, R., Douaik, A., Abdelkrim, D., & Bouabdli, A. (2016). Soil erodibility mapping using three approaches in the Tangiers province–Northern Morocco. *International Soil and Water Conservation Research, 4*(3), 159-167. https://doi.org/10.1016/j.iswcr.2016.07.001

Ishimoto, M. and Iida, K. (1939). Observations of Earthquakes Registered with the Micro Seismograph Constructed Recently. *Bulletin of the Earthquake Research Institute, 17*, 443-478.

Li, R., Zhou, R., & Zhang, J. (2018). Function of PM2.5 in the pathogenesis of lung cancer and chronic airway inflammatory diseases. *Oncology letters, 15(*5), 7506-7514. https://doi.org/10.3892/ol.2018.8355

Kadir, E. A., Kung, H. T., AlMansour, A. A., Irie, H., Rosa, S. L., & Fauzi, S. S. M. (2023). Wildfire hotspots forecasting and mapping for environmental monitoring based on the long short-term memory networks deep learning algorithm. *Environments, 10*(7), 124. https://doi.org/10.3390/environments10070124

Kaiser, J. W., Heil, A., Andreae, M. O., Benedetti, A., Chubarova, N., Jones, L., Morcrette, J.J., Razinger, M., Schultz, M.G., Suttie, M., & Van Der Werf, G. R. (2012). Biomass burning emissions estimated with
a global fire assimilation system based on observed fire radiative power. *Biogeosciences, 9*(1), 527-554. https://doi.org/10.5194/bg-9-527-2012

Khamsiri, S. (2017). *Frequency-size distribution of the craters on moon.* [Master's thesis, Chulalongkorn University]. Chulalongkorn University Intellectual Repository. https://cuir.car.chula.ac.th/handle/123456789/64103

Korontzi, S., McCarty, J., Loboda, T., Kumar, S., & Justice, C. (2006). Global distribution of agricultural fires in croplands from 3 years of Moderate Resolution Imaging Spectroradiometer (MODIS) data. *Global Biogeochemical Cycles, 20*(2). https://doi.org/10.1029/2005GB002529

Kumar, S., & Kumar, A. (2022). Hotspot and trend analysis of forest fires and its relation to climatic factors in the western Himalayas. *Natural Hazards, 114*(3), 3529-3544. https://doi.org/10.1007/s11069-022-05530-5

Miller, M. R., & Newby, D. E. (2020). Air pollution and cardiovascular disease: car sick. *Cardiovascular research, 116*(2), 279-294. https://doi.org/10.1093/cvr/cvz228

Moran, J., NaSuwan, C., & Poocharoen, O. O. (2019). The haze problem in Northern Thailand and policies to combat it: A review. *Environmental Science & Policy, 97*, 1-15. https://doi.org/10.1016/j.envsci.2019.03.016

Nami, M. H., Jaafari, A., Fallah, M., & Nabiuni, S. (2018). Spatial prediction of wildfire probability in the Hyrcanian ecoregion using evidential belief function model and GIS. *International journal of environmental science and technology, 15*, 373-384. https://doi.org/10.1007/s13762-017-1371-6

Nonthapot, S., Sihabutr, C., & Lean, H. H. (2024). The effects of air pollution on tourism in Thailand. *Geo Journal of Tourism and Geosites, 53*(2), 522-527. https://doi.org/10.30892/gtg.53215-1227

Olabarrieta, M., Valle-Levinson, A., Martinez, C. J., Pattiaratchi, C., & Shi, L. (2017). Meteotsunamis in the northeastern Gulf of Mexico and their possible link to El Niño Southern Oscillation. *Natural hazards, 88*, 1325-1346. https://doi.org/10.1007/s11069-017-2922-3

Pacaldo, R. S., Aydin, M., & Amarille, R. K. (2025). Forest fire and aspects showed no significant effects on most mineral soil properties of black pine forests. *CATENA, 250,* 108801. https://doi.org/10.1016/j.catena.2025.108801

Pailoplee, S. (2017). Probabilities of Earthquake Occurrences along the Sumatra-Andaman Subduction Zone. *Open Geosciences, 9*(1), 53-60. https://doi.org/10.1515/geo-2017-0004

Pope Iii, C. A., Burnett, R. T., Thun, M. J., Calle, E. E., Krewski, D., Ito, K., & Thurston, G. D. (2002). Lung cancer, cardiopulmonary mortality, and long-term exposure to fine particulate air pollution. *Jama, 287*(9), 1132-1141. https://doi.org/10.1001/jama.287.9.1132

Prasertwiriya, K. (2020). *Investigation of rainfall amounts in Thailand* [Master's thesis, Chulalongkorn University]. Chulalongkorn University Intellectual Repository. https://cuir.car.chula.ac.th/handle/123456789/78910

Rogers, B. M., Balch, J. K., Goetz, S. J., Lehmann, C. E., & Turetsky, M. (2020). Focus on changing fire regimes: interactions with climate, ecosystems, and society. *Environmental Research Letters, 15*(3), 030201. https://doi.org/10.1088/1748-9326/ab6d3a

Sjöström, J., & Granström, A. (2023). Human activity and demographics drive the fire regime in a highly developed European boreal region. *Fire Safety Journal, 136,* 103743. https://doi.org/10.1016/j.firesaf.2023.103743

Taghizadeh-Hesary, F., & Taghizadeh-Hesary, F. (2020). The impacts of air pollution on health and economy in Southeast Asia. *Energies, 13*(7), 1812. https://doi.org/10.3390/en1307 1812

Vadrevu, K. P., Csiszar, I., Ellicott, E., Giglio, L., Badarinath, K. V. S., Vermote, E., & Justice, C. (2012). Hotspot analysis of vegetation fires and intensity in the Indian region. *IEEE Journal of selected topics in applied Earth Observations and Remote Sensing, 6*(1), 224-238. https://doi.org/10.1109/JSTARS.2012.2210699

Wiemer, S. (2001). A software package to analyze seismicity: ZMAP. Seismological *Research Letters, 72*(3), 373-382. https://doi.org/10.1785/gssrl.72.3.373

Xing, Y. F., Xu, Y. H., Shi, M. H., & Lian, Y. X. (2016). The impact of PM2. 5 on the human respiratory system. *Journal of thoracic disease, 8*(1), E69. https://doi.org/10.3978/j.issn.2072-1439.2016.01.19

Yadav, R., Tripathi, J., Shanker, D., Rastogi, B., Das, M., & Kumar, V. (2011). Probabilities for the occurrences of medium to large earthquakes in northeast India and adjoining region. *Natural Hazards, 56*, 145-167. https://doi.org/10.1007/s11069-010-9557-y

Yang, Y., Zhang, X., & Fu, Y. (2022). Foreign tourists' experiences under air pollution: Evidence from big data. *Tourism Management, 88,* 104423. https://doi.org/10.1016/j.tourman.2021.104423